Imaging Science in Dentistry 2023; 53: 345-53
https://doi.org/10.5624/isd.20230129

Development and validation of a clinical phantom reproducing various lesions for oral and maxillofacial radiology research

Han-Gyeol Yeom[1,2], Jo-Eun Kim[1], Kyung-Hoe Huh[1], Won-Jin Yi[1], Min-Suk Heo[1], Sam-Sun Lee[1,*]

[1]*Department of Oral and Maxillofacial Radiology and Dental Research Institute, School of Dentistry, Seoul National University, Seoul, Korea*
[2]*Department of Oral and Maxillofacial Radiology, School of Dentistry, Wonkwang University, Iksan, Korea*

ABSTRACT

Purpose: The objective of this study was to propose a method for developing a clinical phantom to reproduce various diseases that are clinically prevalent in the field of dentistry. This could facilitate diverse clinical research without unnecessarily exposing patients to radiation.

Materials and Methods: This study utilized a single dry skull, which was visually and radiographically examined to evaluate its condition. Existing lesions on the dry skull were preserved, and other relevant lesions were artificially created as necessary. These lesions were then documented using intraoral radiography and cone-beam computed tomography. Once all pre-existing and reproduced lesions were confirmed by the consensus of 2 oral and maxillofacial radiologists, the skull was embedded in a soft tissue substitute. To validate the process, cone-beam computed tomography scans and panoramic radiographs were obtained of the fabricated phantom. All acquired images were subsequently evaluated.

Results: Most lesions could be identified on panoramic radiographs, although some sialoliths and cracked teeth were confirmed only through cone-beam computed tomographic images. A small gap was observed between the epoxy resin and the bone structures. However, 2 oral and maxillofacial radiologists agreed that this space did not meaningfully impact the interpretation process.

Conclusion: The newly developed phantom has potential for use as a standardized phantom within the dental field. It may be utilized for a variety of imaging studies, not only for optimization purposes, but also for addressing other experimental issues related to both 2- and 3-dimensional diagnostic radiography. ***(Imaging Sci Dent 2023; 53: 345-53)***

KEY WORDS: Phantoms, Imaging; Radiography, Panoramic; Cone-Beam Computed Tomography; Radiography, Dental

Introduction

The exposure protocol for diagnostic radiation must be optimized to achieve both a reduction in dose and satisfactory image quality, adhering to the principle of ALADA (as low as diagnostically acceptable).[1,2] The primary goal of image acquisition using radiological equipment is to facilitate an accurate diagnosis. As such, it is essential to control the amount of radiation exposure provided by the equipment, while concurrently assessing whether the image quality derived from that level of exposure is sufficiently valuable for diagnostic purposes.[3] If a device with very low exposure produces an image of such poor quality that an accurate diagnosis cannot be made, that exposure, no matter how minimal, is considered unnecessary and should be avoided.[4] Therefore, a standardized evaluation to determine whether the image quality obtained from the equipment is suitable for diagnosis is absolutely crucial. However, comparing the diagnostic capabilities of images captured using various radiation devices or exposure protocols is challeng-

This work was supported by a Basic Science Research Program grant through the National Research Foundation of Korea (NRF), funded by the Ministry of Education (grant no. 2020R1I1A3075360). The funder had no role in the study design, data collection, analysis, data interpretation, or writing of the manuscript.
Received June 15, 2023; Revised August 11, 2023; Accepted August 14, 2023
Published online September 25, 2023
*Correspondence to : Prof. Sam-Sun Lee
Department of Oral and Maxillofacial Radiology, School of Dentistry, Seoul National University, 101 Daehak-ro, Jongno-gu, Seoul 03080, Korea
Tel) 82-2-6256-3050, E-mail) raylee@snu.ac.kr

ing because the same condition of the same patient cannot be exposed multiple times.[5] This makes conducting radiological research on precisely controlled clinical images a challenging task. Although laboratory phantoms such as the SedentexCT phantom (Leeds Test Objects Ltd, York, UK) and the DVT phantom (QUART GmbH, Zorneding, Germany) are currently used in the dental field, their clinical relevance remains uncertain. Furthermore, as they do not directly correspond to the characteristics of each oral and maxillofacial lesion,[6] they may not accurately reflect the patient's diagnosis. Therefore, a need exists for a clinical phantom that can indicate the clinical conditions and the presence of common oral and maxillofacial lesions through radiation exposure.[5] By creating a clinical phantom using a real skull on which common lesions of the oral and maxillofacial region are reproduced, the clinical image quality of the radiation equipment can be evaluated without unnecessary patient exposure. This also allows for the comparison of images from various devices under the same clinical conditions.

Several reports have been published on the development and application of numerous phantoms, each reproducing different clinical lesions such as periodontitis,[7-10] dental caries,[11-13] tooth fractures,[14] and external root resorption.[15]

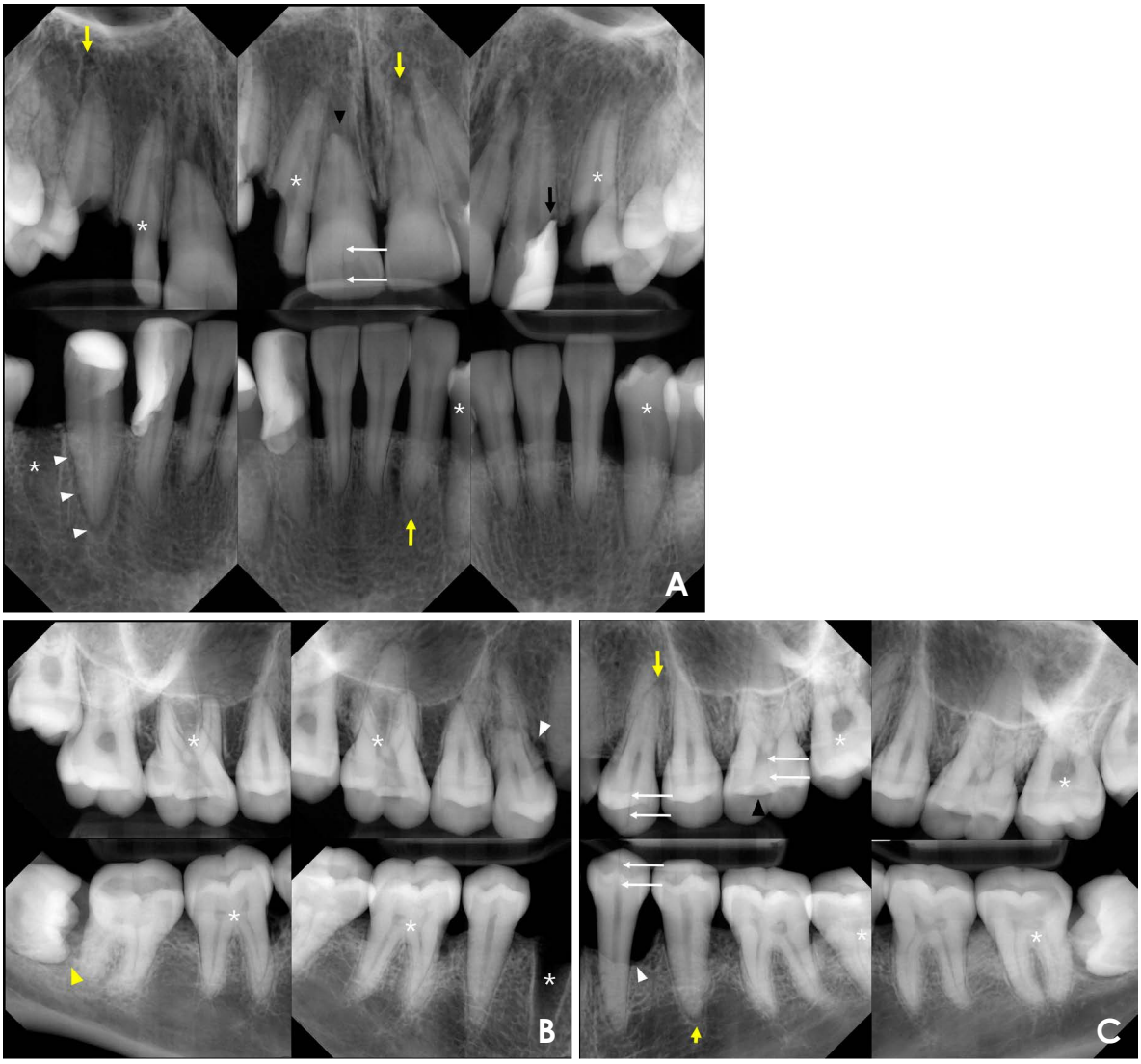

Fig. 1. The lesions present in the dry skull were confirmed using periapical radiographs. *: Following tooth extraction or using an existing extraction socket, a new tooth with reproduced lesions was implanted within the socket. A. Anterior area. Black arrow: secondary caries; white arrow: vertical crack; yellow arrow: periapical periodontal ligament (PDL) space widening or periapical rarefaction; black arrowhead: external root resorption; white arrowhead: periodontal bone loss. B. Right area. White arrowhead: periodontal bone loss; yellow arrowhead: pericoronitis. C. Left area. White arrow: vertical crack; yellow arrow: periapical PDL space widening or periapical rarefaction; white arrowhead: periodontal bone loss; black arrowhead: loss of filling material.

However, to the best of our knowledge, both published reports and commercial products are lacking regarding a universally applicable oral and maxillofacial phantom that accurately simulates multiple diseases and is substantiated by multiple references.

Thus, the objective of the present study was to introduce a method for developing a clinical phantom that can reproduce a range of diseases commonly seen in dental practice. Such a phantom could facilitate diverse clinical research without subjecting patients to unnecessary radiation exposure. Additionally, the phantom created using this method could function as a foundational instrument in various clinical studies of image quality in oral and maxillofacial radiology.

Materials and Methods

Evaluation of natural skull features and reproduction of common oral and maxillofacial pathologies

The skull utilized in this study was previously analyzed and studied for research purposes at the oral and maxillofacial department of Seoul National University, prior to the enactment of the Enforcement Rule of the Bioethics and Safety Act.[16,17] The skull was visually and radiographically examined using periapical radiographs, panoramic radiographs, and cone-beam computed tomography (CBCT) to assess its current condition. The preservation of the skull was satisfactory in terms of bone and dental tissues. Visual inspection revealed some tooth fractures and dental caries, which were subsequently confirmed by radiographic examination. Existing lesions in the dry skull were preserved (Fig. 1), and other common lesions were artificially introduced.

For the study of dental caries, a tooth exhibiting a typical carious shape on an intraoral radiograph was selected from the extracted human teeth that corresponded to the tooth number to be replicated. To simulate periodontitis, a portion of the alveolar bone was removed using one-half and one-quarter round diamond burs (Midwest Once; Dentsply Sirona, Charlotte, NC, USA).[7] To reflect a dens evaginatus, the nodular portion of a tooth with an actual dens evaginatus was accentuated using a flowable resin (Filtek Supreme Flowable Restorative; 3M ESPE, St. Paul, MN, USA), which has an attenuation similar to that of enamel.

A Dentium FX3412 fixture (3.4 mm × 12.0 mm; Dentium, Seoul, Korea) was implanted in the area of the left maxillary first molar to replicate an implant fixture. Horizontal root fracture was simulated by sectioning each tooth, which was accomplished using a single cut from a 100-μm-wide diamond-coated circular saw blade (Isomet 1000; Buehler, Lake Bluff, IL, USA).[14] Visual and radiographic confirmations were obtained using periapical radiographs. For the simulation of external resorption, apical inflammation, and vertical cracks, the original lesions present in the skull were utilized.

Sialoliths of the parotid and submandibular glands were formed using resin blocks and Filtek Z250 (3M ESPE). The sialolith associated with the right parotid gland was situated near the area corresponding to the orifice of the main duct. The sialolith of the left parotid gland was positioned in an area corresponding to the parenchymal region of the gland. The sialoliths of the right and left submandibular glands were placed in the parenchymal and orifice regions of the main duct, respectively. The resin blocks were fixed with epoxy bonds (Masterseal 151; Masterbond Inc, Hackensack, NJ, USA).

To simulate degeneration of the right condyle, bony defects were induced by inserting half of a 1.5 mm-diameter round carbide bur (Midwest Once; Dentsply Sirona) into the lateral pole, mesial pole, and superior region.[18,19] An osteophyte was reproduced using dental material deposited on the anterior margin of the condyle. The specific material was G-FIX (GC Korea, Seoul, Korea), which has an attenuation similar to that of cortical bone (Fig. 2).

A focal defect was engineered in the mandibular cortex, positioned inferiorly to the right second molar of the mandible. This was accomplished using a round bur with a dia-

Fig. 2. An osteophyte was reproduced using G-FIX material (GC Korea, Seoul, Korea) deposited on the anterior margin of the right condyle (white arrowhead).

Table 1. Lesions reproduced on the clinical phantom

Right maxilla		Left maxilla	
Central incisor	External root resorption, vertical crack	Central incisor	Periapical lesion
Lateral incisor*	Secondary caries†, horizontal root fracture†	Lateral incisor	Secondary caries
Canine	Crown fracture with pulp exposure, periapical PDL space widening	Canine*	Rotation†, apical involvement in periodontal bone loss†, vertical crack†
First premolar	Mesial vertical bone loss	First premolar	Vertical crack, periapical PDL space widening
Second premolar	Vertical crack†	Second premolar	Non-specific
First molar*	Multi-surface caries†, periapical lesion†	First molar	Loss of filling material, vertical crack
Second molar	Furcation involvement periodontal bone loss	Second molar*	Implant fixture†
Third molar	Impacted tooth	Third molar	Impacted tooth
Right mandible		Left mandible	
Central incisor	Horizontal bone loss	Central incisor	Horizontal bone loss†, horizontal root fracture†
Lateral incisor	Horizontal bone loss	Lateral incisor	Periapical PDL space widening, horizontal bone loss
Canine	Apical involvement in periodontal bone loss	Canine*	Apical involvement in periodontal bone loss†, enamel dysplasia†, vertical root fracture†
First premolar*	Dens evaginatus†, apical involvement in periodontal bone loss†	First premolar	Vertical crack, distal vertical bone loss
Second premolar	Crown fracture without pulp exposure†	Second premolar	Periapical PDL space widening
First molar*	Horizontal root fracture†, root dilaceration†	First molar	Vertical crack†, furcation involvement periodontal bone loss†
Second molar	Vertical crack	Second molar*	Secondary caries†, attrition†, apical involvement in periodontal bone loss†
Third molar	Impacted tooth, pericoronitis	Third molar	Impacted tooth
Both submandibular glands	Sialolith	Both parotid glands	Sialolith
Right TMJ	Degenerative change	Right mandibular cortex	Cortical defect

*: tooth implanted after tooth extraction or using an existing extraction socket. †: lesions reproduced under the precise methodology described in the main text. PDL: periodontal ligament, TMJ: temporomandibular joint

meter of 1.0 mm (Midwest Once, Dentsply Sirona).

The preserved or reproduced lesions were confirmed through the consensus of 2 oral and maxillofacial radiologists, one with 8 years of experience and the other with over 20 years of experience. Table 1 presents a list of the lesions.

Reproduction of the spine, hyoid bone, and soft tissue

Cervical spine and hyoid bone models (3B Scientific, Tucker, GA, USA) were utilized to reproduce the cervical spine and hyoid bone. Multidetector computed tomography revealed that the radiodensity of the model was approxi-

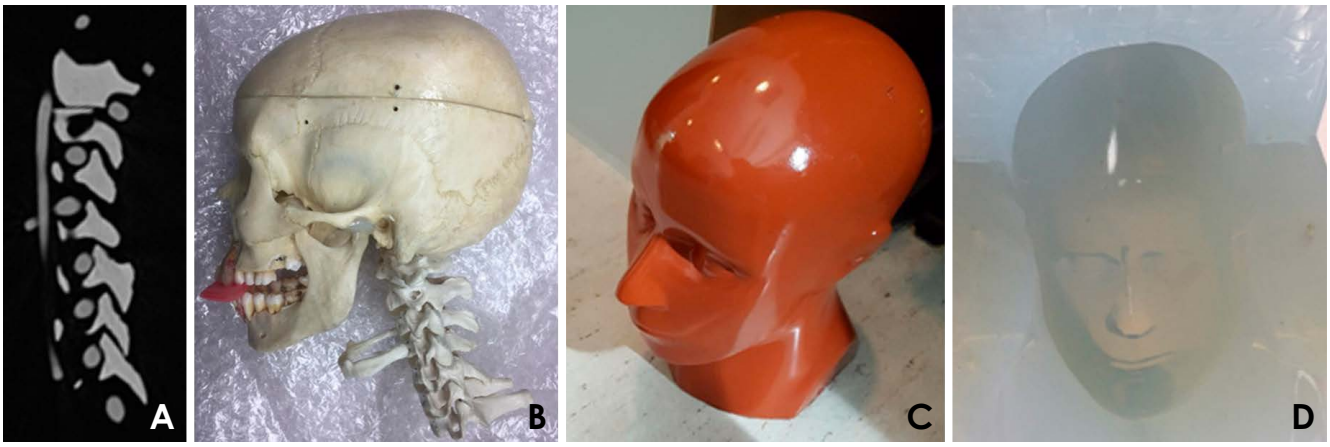

Fig. 3. A. Multidetector computed tomography of the cervical spinal column model reveals that the radiodensity of the model ranged from 1000 to 1250 Hounsfield units (HUs), a value comparable to that of bone. B. The fabricated skull, spine, and hyoid bone were fixed with epoxy bonds prior to the pouring of soft tissue equivalent. C. A female Alderson Rando phantom (Alderson Research Laboratories, Stamford, CT, USA) was utilized to replicate the contours and characteristics of the human face. D. A negative silicone mold was produced using the Alderson Rando phantom as a positive mold.

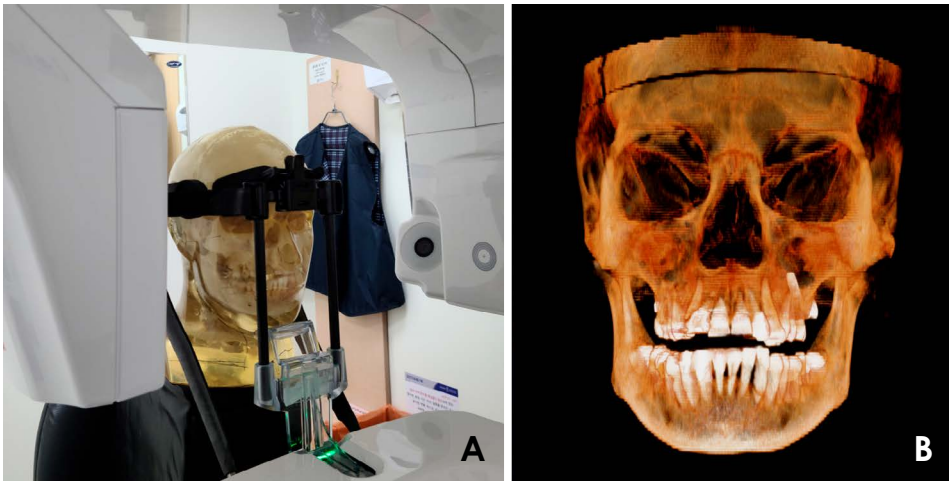

Fig. 4. A. The resulting phantom was scanned using cone-beam computed tomography (CBCT) and panoramic radiography to ensure the successful capture of imaging features, ensuring their similarity to those of actual lesions. B. The acquired 3-dimensional volume rendering of the CBCT image for the phantom.

mately 1000-1250 Hounsfield units (HUs), a value comparable to that of bone (Fig. 3A). The skull, spine, and hyoid bone were fixed with epoxy bonds (Masterseal 151; Masterbond Inc) (Fig. 3B). To simulate the appearance of soft tissue, a ready-made radiation test phantom, specifically a female Alderson Rando phantom (Alderson Research Laboratories, Stamford, CT, USA), was used (Fig. 3C). A negative silicone mold was created using the phantom as a positive mold (Fig. 3D).

The fixed skull, spine, and hyoid bone were centrally positioned within a silicone negative mold. Soft tissue was then simulated by pouring a specific soft tissue material (Neo3010; Neochemo, Gimhae-si, Korea) into the gap between the bone and the external contour of the soft tissue. The selected soft tissue material was an epoxy compound with a density of 80 HU, a value corresponding with the HU value of actual soft tissue. To minimize the formation of air bubbles, the curing process was performed twice.

Acquisition of CBCT and panoramic radiography

For validation, the phantom was scanned using both CBCT and panoramic radiography. This was done to confirm that the imaging features resembled those of actual lesions and to check for the presence of air bubbles, artifacts, and inhomogeneities in the epoxy compound (Fig. 4). CBCT images were acquired using a CS 9600 device (Carestream, Rochester, NY, USA) with a field of view of 170 × 150 mm, a voxel size of 0.15 mm, and a voltage of 120 kV. Digital Imaging and Communications in Medicine files were exported using OnDemand3D version 1.0 (Cybermed,

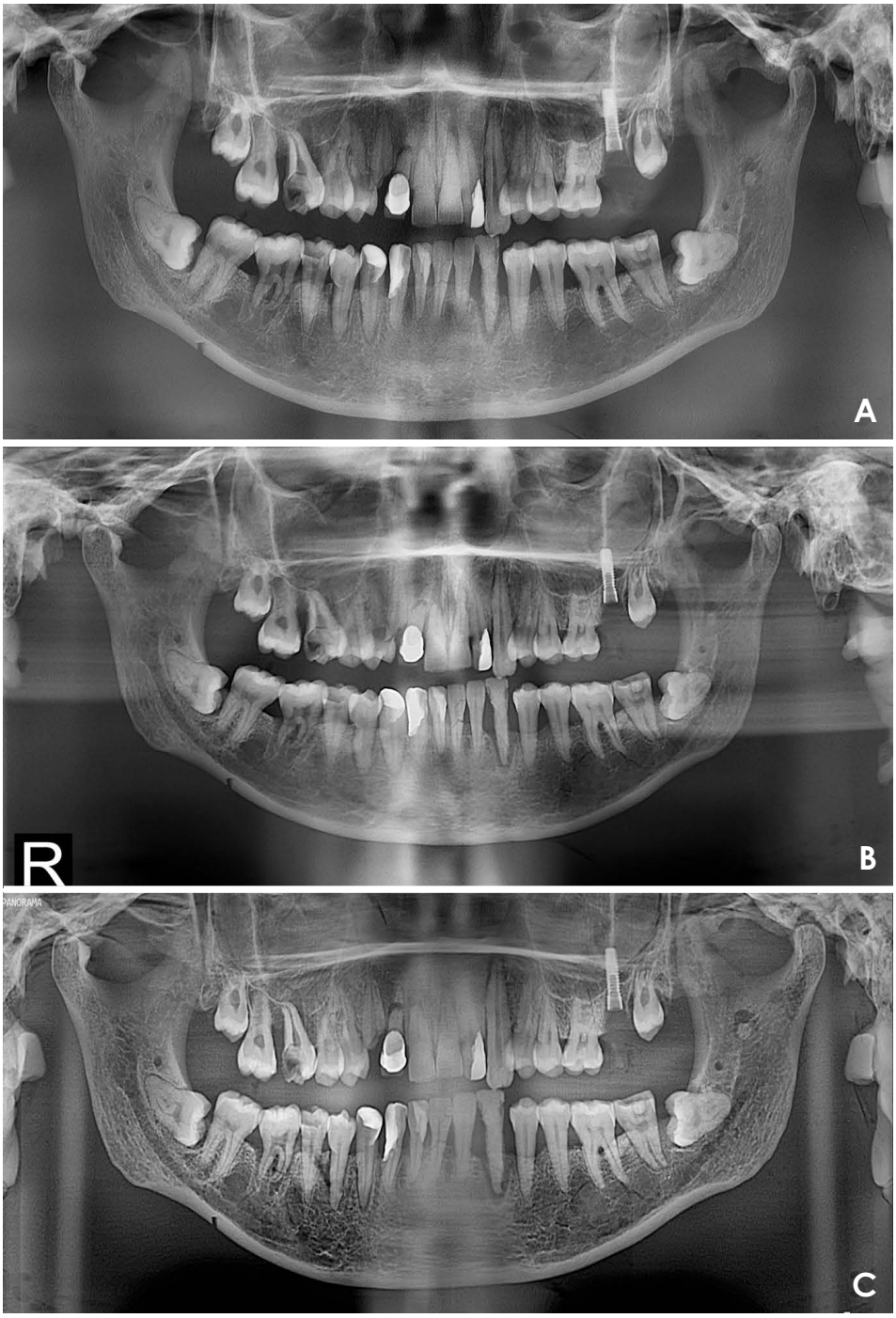

Fig. 5. The panoramic radiographs obtained with the 3 devices provided a high level of diagnostic capability for the lesions. A. PCH-2500 (Vatech, Seoul, Korea). B. T1 (Osstem, Seoul, Korea). C. Eco-X (HDX, Seoul, Korea).

Seoul, Korea). For the panoramic radiographs, PCH-2500 (Vatech, Seoul, Korea), T1 (Osstem, Seoul, Korea), and Eco-X (HDX, Seoul, Korea) devices were used according to the instructions in the user manuals. The settings were as follows: 72 kVp, 10 mA, and 13.5 s for Vatech; 80 kV, 10 mA, and 16 s for Osstem; and 90 kV, 10 mA, and 14 s for HDX (Fig. 5). In the process of obtaining panoramic radiographs from the ideal position, panoramic radiographs from other positions were also used to gather additional radiological information. The images obtained were then interpreted by 2 oral and maxillofacial radiologists, one with 8 years of experience and the other with over 20 years of experience.

Results

Panoramic radiography and CBCT imaging demonstrated high diagnostic capability for the examined lesions. A major-

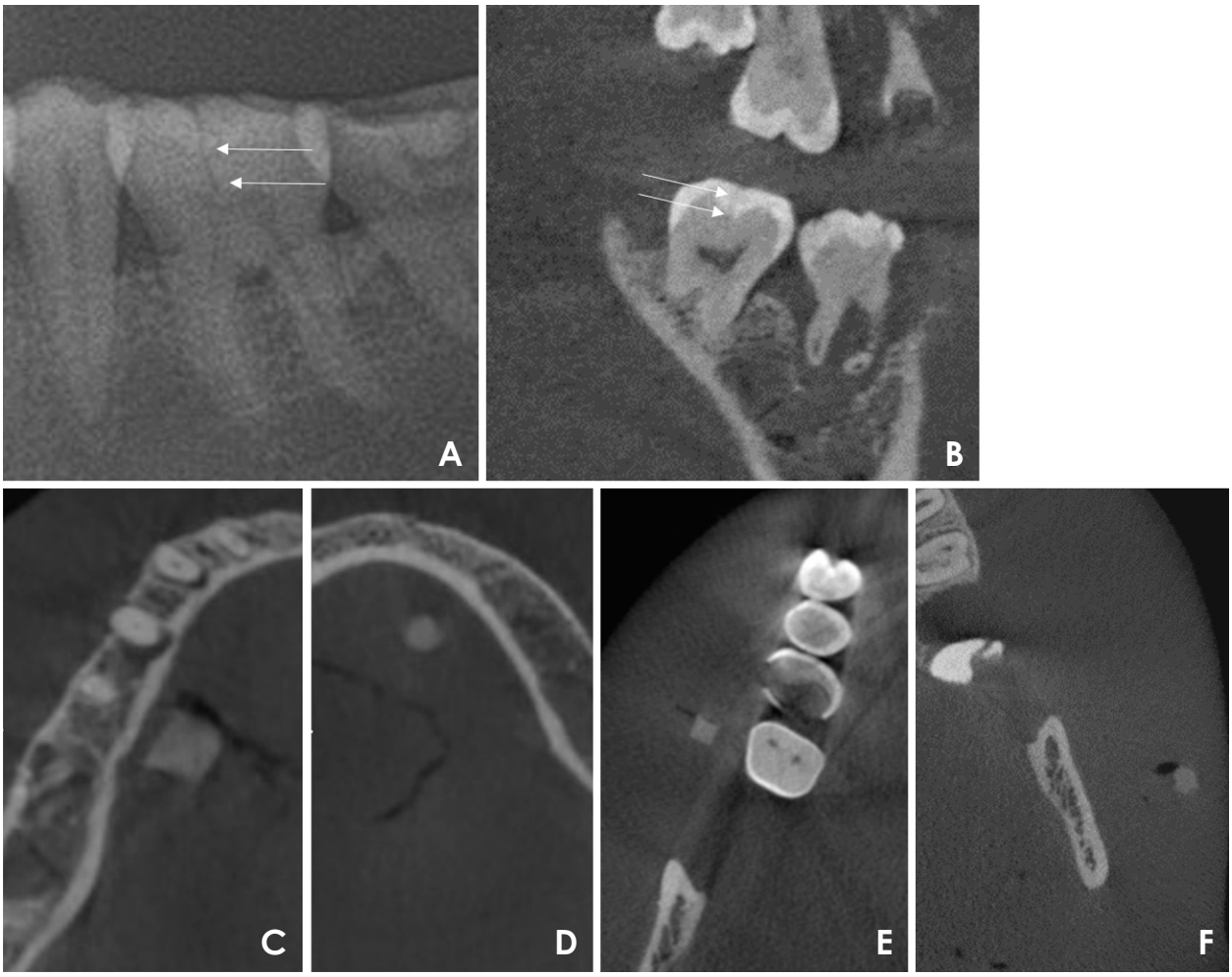

Fig. 6. Lesions that are not readily visible on standard panoramic radiographs can be verified using cone-beam computed tomography (CBCT) or panoramic radiographs taken from different angles. A. A vertical fracture of the mandibular left first molar was verified using a panoramic radiograph taken from a different angle. The white arrow indicates the vertical fracture. B. A vertical fracture in the mandibular right second molar was verified using a CBCT image. The white arrow indicates the vertical fracture. C. A simulated sialolith of the right submandibular gland in the proximal area of the main duct. D. A simulated sialolith of the left submandibular gland in the distal area of the main duct. E. A simulated sialolith of the right parotid gland in the distal area of the main duct. F. A simulated sialolith of the left parotid gland. This sialolith, located in the proximal area of the main duct, is the only one that could be definitively diagnosed using the panoramic radiographs obtained.

ity of the lesions, including dental caries, periapical lesion, periodontal bone loss, implant fixture, mandibular cortex defect, and attrition, were identifiable on the panoramic radiographs (Fig. 5). The vertical crack in the maxillary right second premolar was clearly detected with certain panoramic devices (Figs. 5A and B). However, in the case of the mandibular left first molar and right second molar, the crack lines were not clearly visible on the scans captured with some machines (Fig. 5). Nevertheless, these could be observed on certain panoramic radiographs (Fig. 6A) and CBCT images (Fig. 6B).

The sialoliths formed in the main duct of the left parotid gland were diagnosable on the panoramic radiographs obtained using all 3 devices. However, the sialoliths formed in the right parotid gland and in both submandibular glands were not clearly diagnosable on the panoramic radiographs. All sialoliths were verified using CBCT images (Figs. 6C-F).

The degenerative changes in the right temporomandibular joint were discernible on the panoramic radiographs captured with all 3 devices.

In the CBCT images, a slight space was observed between the epoxy resin and the bone structures. However, the 2 oral and maxillofacial radiologists confirmed that this space did not meaningfully impact the interpretation process.

Discussion

In this radiological study, an *in vitro* phantom was designed to reproduce the conditions of a clinical patient with maximal precision. Previous studies utilizing radiographic imaging of periodontitis have typically involved the arbitrary regeneration of bone loss from dry skull, bovine, or pig bones.[7-10] To simulate periodontal alveolar bone loss, one-half and one-quarter round diamond burs mounted on a high-speed handpiece have generally been used to grind the alveolar bone.[7] This procedure was also employed in the present study to simulate periodontal bone loss.

In the study of dental caries, radiographic phantoms are constructed either by using extracted teeth with existing dental caries or by artificially inducing dental caries to sound extracted teeth.[11-13] Various demineralization buffer systems are employed to generate arbitrary carious lesions. The creation of these artificial lesions is crucial for understanding the mechanisms behind the formation and prevention of dental caries. Consequently, a combination of lesion formation and reversal mechanisms is necessary for the creation of dental caries-like lesions. An accurate study of the formation of dental caries necessitates the use of numerous factors for surface protection. However, radiological studies require a resulting radiolucent condition, which is the only factor that can be detected by radiographic examination. Additionally, when dental caries was reproduced on extracted sound teeth using a reference buffer system during the design phase of the present study, the radiologic imaging features differed from those of typical dental caries. Therefore, extracted teeth with natural carious lesions were used instead.

Jones et al.[18] developed a method for simulating degenerative changes of the condyle. They created small osseous defects in each medial or lateral condylar region using a dental handpiece equipped with a 1.5 mm-diameter round bur. Similarly, Cara et al.[19] used a dental handpiece with a #1014 round bur to simulate lesions. These lesions were approximately the same size as the bur's diameter (1.0 mm) and had a depth equal to half of the diameter of the bur (approximately 0.5 mm). In the present study, bone defects in the condylar region were reproduced in a similar manner.

This study presents an *in vitro* phantom, produced through a complex replication process for various lesions. Although replicating the entire phantom may not be feasible, the production process could serve as a reference for creating diverse clinical phantoms. The proposed phantom holds potential as a standardization tool, providing substantial utility for many imaging studies. The phantom could be employed in numerous studies related to clinical image quality, serving as a valuable instrument. Furthermore, its use could extend beyond optimization, as it could be employed to explore any experimental facets related to 2- and 3-dimensional diagnostic imaging radiography.

Conflicts of Interest: None

References

1. Iskanderani D, Nilsson M, Alstergren P, Shi XQ, Hellen-Halme K. Evaluation of a low-dose protocol for cone beam computed tomography of the temporomandibular joint. Dentomaxillofac Radiol 2020; 49: 20190495.
2. Oenning AC, Pauwels R, Stratis A, De Faria Vasconcelos K, Tijskens E, De Grauwe A, et al. Halve the dose while maintaining image quality in paediatric cone Beam CT. Sci Rep 2019; 9: 5521.
3. Martin CJ, Sharp PF, Sutton DG. Measurement of image quality in diagnostic radiology. Appl Radiat Isot 1999; 50: 21-38.
4. Uffmann M, Schaefer-Prokop C. Digital radiography: the balance between image quality and required radiation dose. Eur J Radiol 2009; 72: 202-8.
5. Oenning AC, Salmon B, Vasconcelos KF, Pinheiro Nicolielo LF, Lambrichts I, Sanderink G, et al. DIMITRA paediatric skull phantoms: development of age-specific paediatric models for dentomaxillofacial radiology research. Dentomaxillofac Radiol 2018; 47: 20170285.
6. Choi JW, Lee SS, Choi SC, Heo MS, Huh KH, Yi WJ, et al. Relationship between physical factors and subjective image quality of cone-beam computed tomography images according to diagnostic task. Oral Surg Oral Med Oral Pathol Oral Radiol 2015; 119: 357-65.
7. Bayat S, Talaeipour AR, Sarlati F. Detection of simulated periodontal defects using cone-beam CT and digital intraoral radiography. Dentomaxillofac Radiol 2016; 45: 20160030.
8. Ramesh A, Ludlow JB, Webber RL, Tyndall DA, Paquette D. Evaluation of tuned-aperture computed tomography in the detection of simulated periodontal defects. Oral Surg Oral Med Oral Pathol Oral Radiol Endod 2002; 93: 341-9.
9. Bagis N, Kolsuz ME, Kursun S, Orhan K. Comparison of intraoral radiography and cone-beam computed tomography for the detection of periodontal defects: an in vitro study. BMC Oral Health 2015; 15: 64.
10. Vandenberghe B, Jacobs R, Yang J. Detection of periodontal bone loss using digital intraoral and cone beam computed tomography images: an in vitro assessment of bony and/or infrabony defects. Dentomaxillofac Radiol 2008; 37: 252-60.
11. Countryman SC, Sousa Melo SL, Belem MDF, Haiter-Neto F, Vargas MA, Allareddy V. Performance of 5 different displays in the detection of artificial incipient and recurrent caries-like lesions. Oral Surg Oral Med Oral Pathol Oral Radiol 2018; 125: 182-91.
12. Sousa Melo SL, Belem MD, Prieto LT, Tabchoury CP, Haiter-Neto F. Comparison of cone beam computed tomography and digital intraoral radiography performance in the detection of

artificially induced recurrent caries-like lesions. Oral Surg Oral Med Oral Pathol Oral Radiol 2017; 124: 306-14.
13. Abu El-Ela WH, Farid MM, Mostafa MS. Intraoral versus extraoral bitewing radiography in detection of enamel proximal caries: an ex vivo study. Dentomaxillofac Radiol 2016; 45: 20150326.
14. Jones D, Mannocci F, Andiappan M, Brown J, Patel S. The effect of alteration of the exposure parameters of a cone-beam computed tomographic scan on the diagnosis of simulated horizontal root fractures. J Endod 2015; 41: 520-5.
15. Goller Bulut D, Uğur Aydın Z. The impact of different voxels and exposure parameters of CBCT for the assessment of external root resorptions: a phantom study. Aust Endod J 2019; 45: 146-53.
16. Lee KH, Lee SB, An CH, Heo MS, Yi WJ, Huh KH, et al. The influence of X ray beam angulation on the fractal analysis of trabecular architecture in human dry mandible using standardized tile counting method. Korean J Oral Maxillofac Radiol 2004; 34: 179-83.
17. Kim MJ, Choi BR, Huh KH, Yi WJ, Heo MS, Lee SS, et al. Comparison of measurements from digital cephalometric radiographs and 3D MDCT-synthetized cephalometric radiographs and the effect of head position. Korean J Oral Maxillofac Radiol 2009; 39: 133-47.
18. Jones EM, Papio M, Tee BC, Beck FM, Fields HW, Sun Z. Comparison of cone-beam computed tomography with multislice computed tomography in detection of small osseous condylar defects. Am J Orthod Dentofacial Orthop 2016; 150: 130-9.
19. Cara ACB, Gaia BF, Perrella A, Oliveira JXO, Lopes PML, Cavalcanti MGP. Validity of single- and multislice CT for assessment of mandibular condyle lesions. Dentomaxillofac Radiol 2007; 36: 24-7.